Ultrasonics Sonochemistry 19 (2012) 209–215

Contents lists available at ScienceDirect

Ultrasonics Sonochemistry

journal homepage: www.elsevier.com/locate/ultsonch

A novel polyol method to synthesize colloidal silver nanoparticles by ultrasonic irradiation

Jeong Hoon Byeon [a], Young-Woo Kim [b,*]

[a] Department of Chemistry, Purdue University, IN 47907, USA
[b] Department of Automotive Engineering, Hoseo University, Asan 336-795, Republic of Korea

ARTICLE INFO

Article history:
Received 13 February 2011
Received in revised form 30 May 2011
Accepted 6 June 2011
Available online 15 June 2011

Keywords:
Polyol synthesis
Silver nanoparticles
Ultrasonic irradiation
Uniform mixing

ABSTRACT

A polyol synthesis of silver nanoparticles in the presence of ultrasonic irradiation was compared with other configurations (at ambient temperature, 120 °C, and 120 °C with injected solutions) in the absence of ultrasonic irradiation in order to obtain systematic results for morphology and size distribution. For applying ultrasonic irradiation, rather fine and uniform spherical silver particles (21 ± 3.7 nm) were obtained in a simple (at ambient temperature without mechanical stirring) and fast (within 4 min, 3.61×10^{-3} mol min^{-1}) manner than other cases (at ambient temperature (for 8 h, 0.03×10^{-3} mol min^{-1}): 86 ± 16.8 nm, 120 °C (for 12 min, 1.16×10^{-3} mol min^{-1}): 64 ± 14.9 nm, and 120 °C with injected solutions (during 12 min): 35 ± 6.8 nm; all other cases contained anisotropic shaped particles). Even though the temperature of polyol reaction reached only at 80 °C (<120 °C) in the presence of ultrasonic irradiation, a uniform mixing (i.e. enhanced collision between silver particle and surrounding components) by ultrasonic irradiation might induce a better formation kinetics and morphological uniformity.

1. Introduction

Metal nanoparticles have attracted considerable interest in various fields of chemistry due to their novel physicochemical properties differing significantly from macroscopic metal phases [1]. For example, they can serve as a model system to experimentally probe the effects of quantum confinement on electronic, magnetic, and other properties [2,3]. They have also been widely exploited for use in photography, catalysis, biological labeling, photonics, optoelectronics, information storage, surface-enhanced Raman scattering (SERS), and the formulation of magnetic ferrofluids [4]. The intrinsic properties of metal nanoparticles are mainly determined by their size, shape, composition, crystallinity, and structure. The design of a generic method for the preparation of metal nanoparticles with a broad range of well-defined and controllable morphologies is still needed in order to fully exploit their peculiar properties and unique applications [5–8].

Among the metal nanoparticles, silver nanoparticles have been widely investigated [2,7,9–11] because they exhibit unusual optical, electronic, and chemical properties, depending on their size and shape, thus opening many possibilities with respect to technological applications, such as antibacterial materials, antistatic materials, cryogenic superconducting materials, biosensor materials, etc. [12]. The chemical reduction method is one of the most common methods to synthesize colloidal silver nanoparticles, because of its convenience and the simple equipment needed [13]. The synthesis method used in the present study is the so-called polyol method, which is well suited for the preparation of metal or oxide nanoparticles of various shapes [14,15]. The general polyol process involves the dissolution of a silver precursor and a protecting agent or stabilizer in a polyol medium.

The chemical effects of ultrasonic irradiation are due to the very high temperature and pressure that are transiently formed (sub-μs) in collapsing bubbles [9,16,17], which have successfully increased the conversion, improved the yield, changed the reaction pathway, and/or initiated the reaction in biological, (electro)chemical, and even for aerosol systems [18,19]. Today in the ultrasonic assisted synthesis of nanoparticles it has been found that ultrasonic irradiation may affect the size distribution of the particles in a narrower range than conventional heating by thermal convection, because of the penetration property of ultrasonic irradiation through solution, resulting in a uniform activation energy for the reaction solution. Moreover, compared to the microwave synthesis of silver nanoparticles [20], the ultrasonic synthesis also can control the morphology and size distribution of the nanoparticles; little is known about influence of ultrasonic irradiation during polyol synthesis.

In this paper, the formation of particles by irradiation of ultrasonic (case D) was compared with other polyol configurations (at ambient temperature for case A, at 120 °C for case B, and at 120 °C with injected solutions for case C) under an identical polyol

* Corresponding author. Tel.: +82 41 540 5819; fax: +82 41 540 5818.
E-mail address: ywkim@hoseo.edu (Y.-W. Kim).

1350-4177/$ - see front matter © 2011 Elsevier B.V. All rights reserved.
doi:10.1016/j.ultsonch.2011.06.004

solution in order to obtain systematic results regarding the formation of colloidal silver nanoparticles. In particular, for the ultrasonic irradiation (case D), the ambient temperature without additional stirring adopted to the polyol solution because the temperature and stirring had little effect on the formation of the metal nanoparticles, which might be due to the fact of the strong penetration property of the ultrasonic irradiation through the solution [18,21].

2. Materials and methods

The polyol solution was a mixture of solutions 1 and 2 at a 1:5 (v/v) ratio. Eighty-five milligrams of silver nitrate (SN, 99.9%, Aldrich), used as a precursor of silver, was dissolved in 5 mL of deionized water (DW) (Solution 1). Two grams of polyvinylpyrrolidone (PVP, M_w = 10,000, Aldrich), used as a protecting agent or stabilizing agent, dissolved in 25 mL of ethylene glycol (EG, 99.9%, Aldrich, US) (Solution 2). All the chemicals used in the polyol configurations (cases A–D) were identical to those described above.

In cases A (Fig. 1a) and B (Fig. 1b), the solutions 1 and 2 mixed and stirred in a flask left at an ambient temperature (A) or fitted in an oil bath heated up to 120 °C (B). Case C (Fig. 1c) was identical to B except for an injection of solutions 1 and 2. Solutions 1 and 2 were injected drop by drop with the aid of a peristaltic pump (323Du/MC4, Watson-Marlow Bredel Pump, US) at constant rates of 0.42 and 2.08 mL/min, respectively. In the D case (Fig. 1d), which is adapted from the so-called Branson sonochemical reactor, solutions 1 and 2 mixed in a flask and then an ultrasonic probe (VCX 750, 13 mm titanium alloy horn, 20 kHz, Sonics & Materials Inc., US) was immersed into the mixture solution. The probe acted as an ultrasonic irradiator (10 W mL^{-1} input power density) and the active part of the probe was the planar circular surface, of area 1.3 cm^2, at the bottom of the probe. Upon the start of reactions, the pale yellow solution changed to dark brown indicating the formation of particles. At the end of the reaction period, the dispersion was cooled in tap water until the system reached the ambient temperature. The particles were separated from the dispersion after the addition of a large amount of acetone followed by centrifugation (for an effective separation of silver particles) for 30 min. The precipitated particles, which were redispersed in ethanol, were used for the characterization studies.

In order to analyze the conversion (reduction of silver ions) of the polyol method, we used a microfiltration membrane (0.2 μm pore size, 11807-47-N, Sartorius, Germany) to separate the particles from the dispersion. The clear filtrate was then analyzed for residual silver content by inductively coupled plasma-atomic emission spectroscopy (ICP-AES; Elan 6000, Perkin-Elmer, US).

A drop of the dispersion was placed on a carbon-coated copper grid, which was allowed to dry before being used for observation following microscopy analyses. The surface morphology and chemistry of the particles were obtained by field-emission scanning electron microscopy (FESEM; JSM-6500F, JEOL, Japan) and energy dispersive X-ray spectroscopy (EDX; JED-2300, JEOL, Japan) at an accelerating voltage of 15 kV. The morphology and microstructure of the particles were analyzed using high-resolution transmission electron microscopy (HRTEM; JEM-3010, JEOL, Japan) in a bright field mode operated at 300 kV. The average particle size and the size distribution of the particles were obtained by image analysis of the micrographs of the particles. The size distributions of the particles were obtained by measuring the diameter D_i of each particle from four micrographs on different parts of the grid. Depending on the reaction configuration, the number of particles, n, ranged from 50 to 200. The standard deviation, σ, was calculated from the following equation:

$$\sigma = \left\{ \left[\sum n(D_i - D)^2 \right] \Big/ [n-1] \right\}^{1/2} \quad (1)$$

where D is the average diameter.

The sample for X-ray photoelectron spectroscopy (XPS) characterization was prepared by placing 50 μL of the dispersion on a glass slide and examining it on an ESCLAB MKII (UK). The optical properties of the dispersions were investigated by ultraviolet–visible (UV–vis) spectroscopy. Absorption spectra were recorded with a Perkin-Elmer 330 spectrophotometer (US), with a variable radiation wavenumber between 300 and 800 nm, at a rate of 60 nm/min

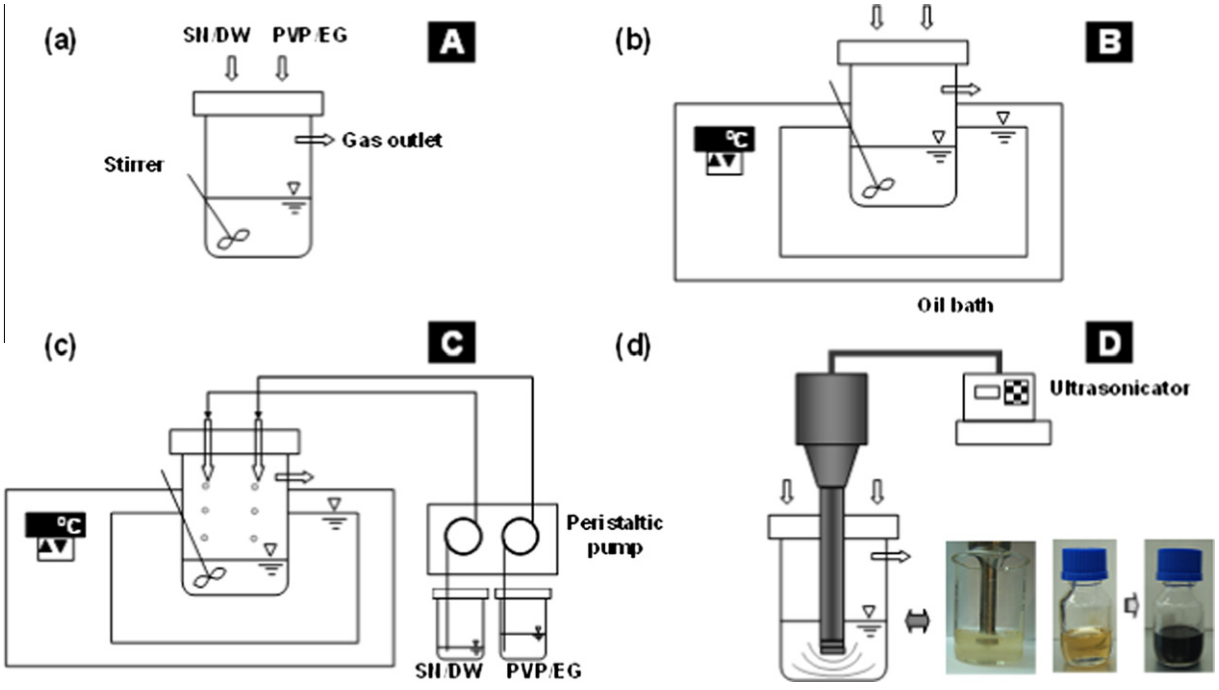

Fig. 1. Polyol configurations of: (a) A, at ambient temperature; (b) B, at 120 °C; (c) C, at 120 °C with injected solutions; and (d) D, for ultrasonic irradiation.

and a spectral resolution of 2 nm. Quartz cells with a path length of 1 cm were used. The crystalline phases of the particles were examined by wide-angle X-ray diffractometry (XRD) on a Rigaku Model D/MAX-Rint 2000 (Japan) diffraction meter using CuKα radiation (λ = 0.15418 nm) at 30 kV and 20 mA. The dried particles were placed onto an oriented monocrystalline quartz plate and scanned from 10° to 100° (2θ) at 4°/min. A mathematical analysis of the Bragg's peaks was undertaken to calculate the crystallite size using the Scherrer formula,

$$t = k\lambda/\beta\cos\theta \quad (2)$$

where t is the crystallite size, k is a constant (=0.9 assuming that the particles are spherical), λ is the wavelength of the X-ray radiation, β is the line width (obtained after correcting for the instrumental broadening), and θ is the angle of diffraction. The surface area of the particles was measured using a porosimeter (ASAP 2010, Micromeritics Ins. Corp., US) at −196 °C with relative pressures ranging from 10^{-6} to 1. High purity (99.9999%) nitrogen gas was used as the adsorbent. The specific surface area was determined using the Brunauer, Emmett, and Teller (BET) equation [22].

3. Results and discussion

Upon the mixing of solutions 1 and 2, the soluble silver ions were reduced to atoms that grow particles. In our experiments, the silver ions could be reduced by both EG and PVP. The general mechanism of reduction of silver ions by EG is represented by following reactions [23,24]:

$$CH_2OH{-}CH_2OH \rightarrow CH_3CHO + H_2O \quad (3)$$

$$2CH_3CHO + 2Ag^+ \rightarrow 2Ag + 2H^+ + CH_3COCOCH_3 \quad (4)$$

The formation of silver particles in EG in the absence of PVP might occur through reactions (Eqs. (3) and (4)). The analysis of EG after the reaction by ^{1}H nuclear magnetic resonance (NMR, Inova-300, Varian, US) revealed that a peak appeared at ~4.2 ppm. The new peak at ~4.2 ppm might be attributed to the formation of aldehyde during the reduction of silver ions, which will cause a downfield shift of the methylene connected to aldehyde [23]. Since the nitrogen and oxygen in the polar group of PVP have a strong coordinative field, the coordinative complex between silver ions and PVP could be formed. Here correspondingly, PVP reacted with the silver ions, in which silver ions might receive electronic clouds from the ligand of —N and C=O in pyrrolidone rings to reduce the silver atoms [4,13,25]. As the reactions proceed, the concentration of silver atoms reached a critical concentration for nucleation. When nucleation occurs, some silver atoms convert to nuclei and then grow by deposition of metallic silver until the system reaches the saturation concentration. At the end of the process, silver particles have grown with an individual morphology and the system exhibits a size distribution [12].

The polyol process times to reduce 90% silver ions which were applied were 8 h, 12 min, and 4 min for cases A, B, and D, respectively. By reason of an appropriate comparison, for case C, the injection time of the solutions was set at 12 min (identical to case B). An initial silver ion concentration (~1.7×10^{-2} mol dm^{-3}) for cases B and D rather drastically decreased (~1.7×10^{-3} mol dm^{-3}) as function of reaction time than that for case A, as shown in Fig. 2a. To prepare a baseline among the polyol configurations, the optical properties of dispersions at different stages of each process were investigated by UV–vis spectroscopy. The comparison between the processes was considered for a 90% reduction. It is important that for a 90% reduction of silver ions, the absorbance curve reaches a plateau. The reduction yields of the configurations were estimated using the mass of precipitated particles in each predetermined (90%) amount of silver ions which yielded colloidal particles. At the ambient temperature (case A), however, the kinetics of the process was the slowest (8 h). In case B, the system was heated up to 120 °C and was allowed to equilibrate at this configuration for 12 min. In comparison with cases A and B, the kinetics was the fastest for the case D. This result might have originated from an effect of ultrasonic irradiation resulting in the electrons easily transferring from EG or PVP to silver ions. To verify the reaction kinetics, an estimation was performed using following equation [26,27]:

$$\dot{N} = A\exp\left[-\frac{\Delta G_c}{kT}\right] = A\exp\left[\frac{16\pi\gamma^3 V_m^2}{3k^3T^3N_A^2(\ln S)^2}\right] \quad (5)$$

where $\dot{N}$ is the particle formation rate, A is the Arrhenius parameter, ΔG_c is the critical free energy, k is the Boltzmann constant, T is the reaction temperature, γ is the surface free energy per unit area, V_m is the molar volume, N_A is the Avogadro's constant, and S is the solution with supersaturation. However, some experimental results were not matched well with the estimations, i.e. the particle formation rate for case D was lower than that for case B owing to its lower reaction temperature (reached at 80 °C for case D <120 °C for case B) and higher ln$S$ (1.1 times higher than that for case B). The lower

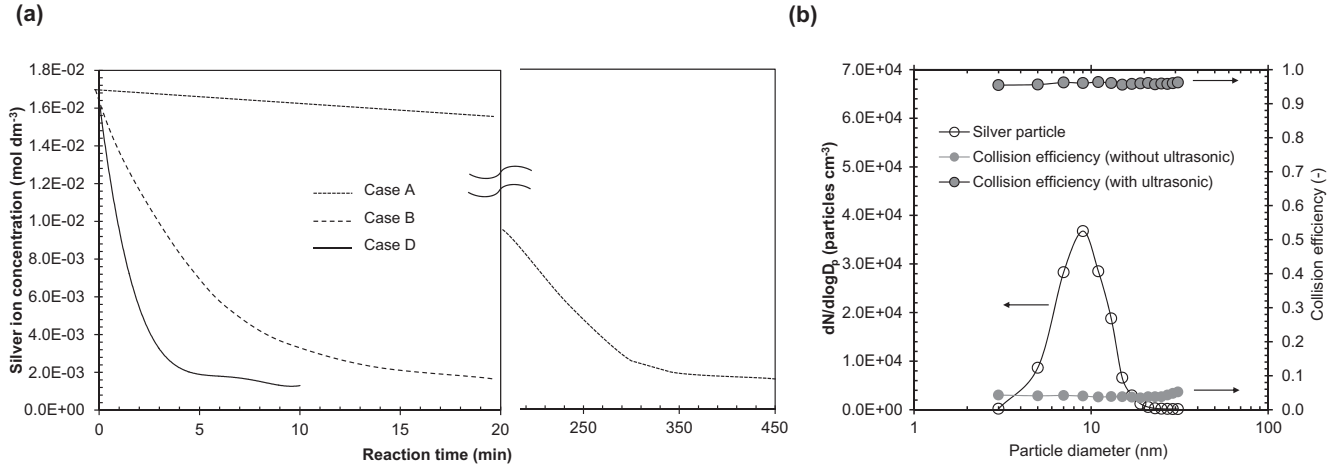

Fig. 2. (a) Changes in the silver ion concentration as a function of reaction time. (b) Results for collision between silver particle and surrounding solution.

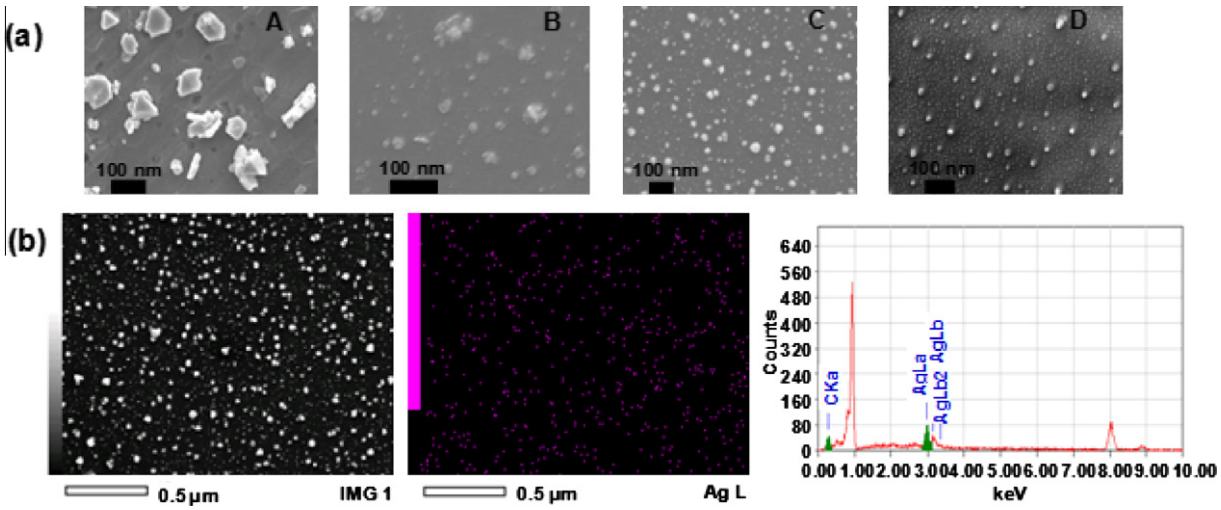

Fig. 3. SEM micrographs (a) of polyol configurations and (b) results of the EDX map and spectrum for case C.

temperature is corresponded to previous report [18], which described that the mechanical effect (shock wave, dispersion, etc.) is predominant in the present ultrasound frequency (20 kHz) irradiation and thermally enhanced nucleation is corresponded to higher frequencies (>100 kHz).

To clarify mechanical effect in the present experiments, more tests were designed and performed in terms of collision efficiency ($\eta_{coll}(d)$, Eq. (6), where, $C_0(d)$ and $C_i(d)$ are the concentrations of injected and collided silver particles, respectively, and measured using a scanning mobility particle sizer (3936, TSI Inc., US)) between silver particle and surrounding components in solution. Silver particles (~10 nm in geometric mean diameter) laden gas was injected into polyol solution without and with ultrasonic irradiation. The resulted efficiencies for without and with ultrasonic irradiation were 0.047 and 0.963, respectively, as shown in Fig. 2b. This means that the reaction opportunity for the presence of ultrasonic irradiation is about 20 times higher than that for the absence of ultrasonic irradiation in a microscopic mechanical aspect [19], and therefore, this might affect the enhancement of the reaction kinetics.

$$\eta_{coll}(d) \propto 1 - \frac{C_i(d)}{C_0(d)} \tag{6}$$

Fig. 3a shows surface morphologies of polyol synthesized particles for each configuration. Anisotropic particles including aggregates were mainly distributed in cases A and B, and the case of A contained a large amount of flake-like particles. In contrast, cases C and D contained spherical particles having a smaller size and a higher morphological uniformity than those in A and B. The first image in Fig. 3b shows a different scaled SEM micrograph of the first image. The dots on the map indicate the positions of elemental silver in the first image, which shows that the polyol configurations produced metallic silver particles. The spectrum shows peaks of binding energies of 2.98, 3.18, and 3.40 keV belonging to Ag $L_{\alpha 1}$, Ag $L_{\beta 1}$, and Ag $L_{\beta 2.15}$, respectively. In addition, the peaks situated at 8.06 and 8.94 keV corresponded to the binding energies of Cu K_α and Cu K_β, respectively, which were derived from the copper grid used for the observations. Throughout the whole scanning range of binding energies, there were no obvious peaks belonging to impurities, which indicated the as-synthesized products were of high purity. Fig. 4 shows the XPS profile corresponding to the Ag 3d spectrum region of the particles. Two peaks were observed at the binding energies of 368.2 and 374.2 eV, corresponding to the Ag $3d_{3/2}$ and Ag $3d_{5/2}$ spectrum regions, respectively, further indicating the formation of metallic silver.

Fig. 5a–d show TEM micrographs having low and high magnitudes and corresponding electron diffraction (ED) patterns. The size distributions were given by the corresponding histograms. The particle morphologies of each configuration corresponded to SEM micrographs (Fig. 3a), and the particle sizes were 86 ± 16.8, 64 ± 14.9, 35 ± 6.8, and 21 ± 3.7 nm for cases A, B, C, and D, respectively. The number density of particles varied with the configurations and the value of case D was the highest which correlated with Eq. (7):

$$n = 6m_{Ag}/\pi d^3 \rho_{Ag} \tag{7}$$

where n is the number of silver particles, m_{Ag} is the mass (10 mg) of silver measured using ICP-AES analysis, d is the average particle diameter from the TEM analyses, and ρ_{Ag} is the bulk density of silver (10.49 g/cm^3). The estimated numbers of silver particles were 0.03, 0.07, 0.42, and 1.90 × 10^{14} for cases A, B, C, and D, respectively.

As illustrated in Fig. 5a, the final product mainly consisted of flake-like particles including triangular shapes, pentagonal shapes, etc. These particles might have came from a shape evolution or transformation process of small silver particles (<50 nm) formed

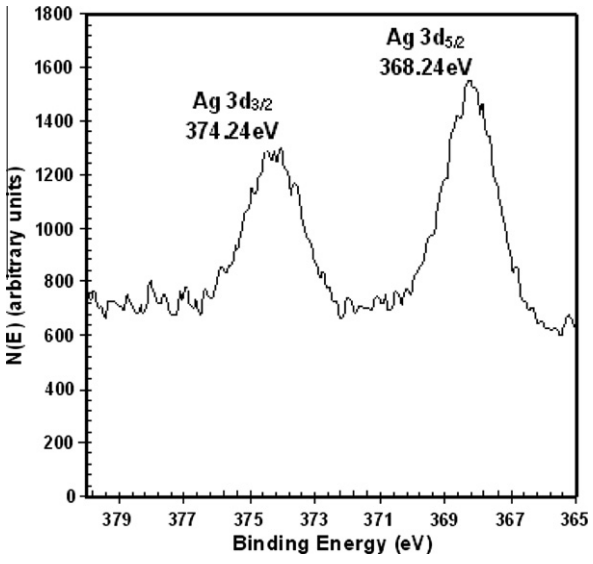

Fig. 4. XPS profile of the synthesized particles.

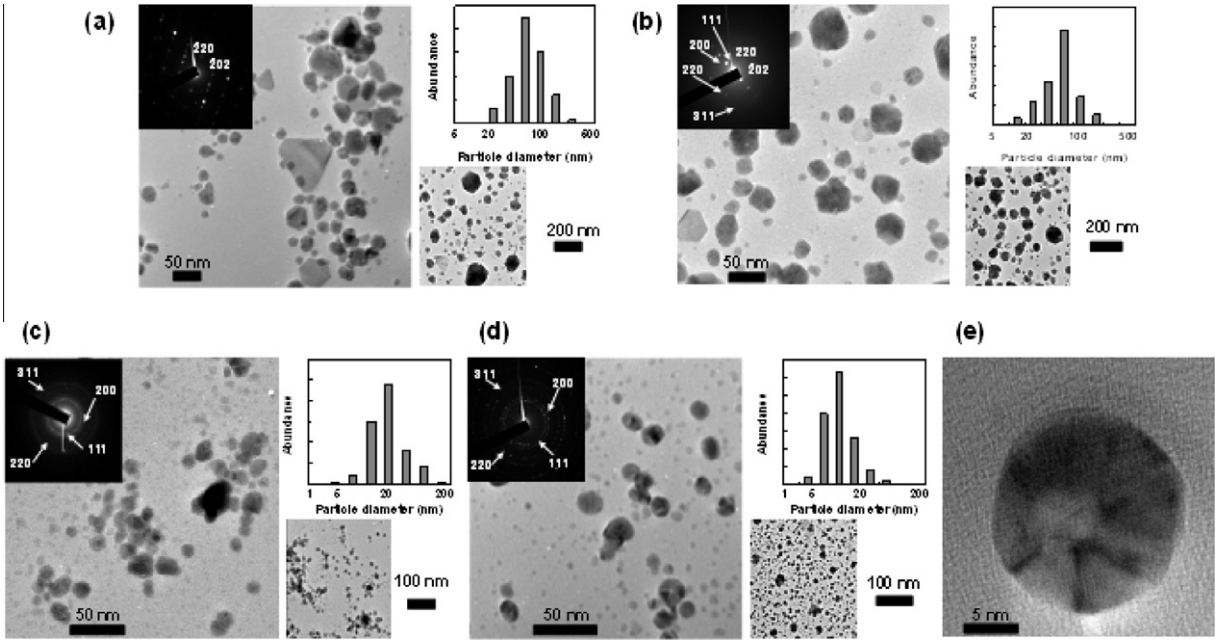

Fig. 5. TEM micrographs, ED patterns, and particle size distributions of cases (a) A, (b) B, (c) C, and (d) D. (e) High magnitude TEM micrograph of a single particle in case D.

at the early stage of the process, which corroborates the observations of other researchers [28–31]. Specifically, it is generally acceptable that PVP molecules can chemically absorb onto the surface of the small silver particles [32] and thus can kinetically control the growth rates of various crystal planes by interacting with the planes of the small particles through adsorption and desorption even at ambient temperature [33]. Adsorbed by PVP molecules, the growth of the (1 1 1) planes was limited, leading to the formation of silver flakes in polygonal shapes and with (1 1 1) crystal planes as their basal plane. In addition, the slow dissolution of the small particles due to a slow kinetics into the solution might also play a certain role in achieving the transformation to the larger particles [34,35]. In case B (Fig. 5b), the product was also dominated by anisotropic particles still having large sizes, even when the reaction was carried out only for 12 min due to a high temperature (120 °C). Because of the high temperature used in B, Brownian motion and the mobility of the surface atoms of the small particles increased despite the existence of the PVP molecules, thus enhancing the probability of particle collision, adhesion, and subsequent coalescence by sintering [36]. The particle coalescence by sintering was the means by which the system tried to attain thermodynamic equilibrium by reducing its total surface area. Some small particles (~20 nm) were also observed in B, which were probably formed via a second round of nucleation [37]. In addition, a few flat polygonal particles in B might have originated from local growth during the process, similar to A. The application of injected solutions (case C, Fig. 5c) exhibited a significant influence on the uniformity of particle morphology and size distribution. It can be seen that the particles were quite spherical and well dispersed. Upon C, a few nuclei form and stable nuclei grow over the time that solutions 1 and 2 were continuously injected into a flask fitted in an oil bath. This configuration helped in lowering the degree of sintering of the product, however, this also proved to be unsatisfactory for complete prevention of particle sintering. It is suggested that some of the silver ions in injected solution 1 were converted to nuclei in the mixture solution and some might be used for growing pre-existing nuclei. Eventually, some sintered particles with larger sizes resulted. In D (Fig. 5d), the uniformity of particle morphology and size distribution was better than in the case of C. As described earlier, the ultrasonic irradiation induced extremely high temperature and pressure at the center of the collapsed bubble and led to enhance chemical reactivities [37]. Even though the intensity of the ultrasonic irradiation used in the present work was not varied, we found that it had reaction accelerating and solution homogenizing effects on the formation of silver particles. Therefore, a steady growth of the particles within this environment produced relatively monodisperse dispersion. In addition, the above effects could also enhance the steric influence against agglomeration and the small silver particles could be effectively separated from each other by PVP. Fig. 5e shows a single silver particle, while in Fig. 5d, the shape was polyhedral and it is possible to observe that the particle was multiply twinned and could be represented schematically as a decahedron having darker triangular contrasts within the particle. The profiles of the particles appeared to be closely spherical.

The structure information of the silver particles was confirmed by ED and the insets of the TEM micrographs (Fig. 5a–d) showed the ED patterns obtained when the electron beam was directed perpendicular to the face of the particles. The ED pattern in Fig. 5a could be easily obtained from anisotropic particles, the strongest intensity spots corresponded to Bragg diffractions from $(\bar{2}20)$ and $(\bar{2}02)$ lattice planes of single crystalline silver. This structure feature was quite common for flake-like metal particles with face-centered cubic (fcc) crystal structures, and similar structure configuration results have also been reported by Wang et al. [28]. The ED pattern in Fig. 5b contained an interpenetrated set of individual diffraction patterns: weak $(\bar{2}20)$ and $(\bar{2}02)$ reflections could be matched to single crystalline silver particles, and weak (1 1 1), (2 0 0), (2 2 0), and (3 1 1) Debye-Scherrer rings could be matched to polycrystalline silver particles. The ED patterns in Fig. 5c–d revealed characteristic rings in a polycrystalline diffraction pattern. Spacing was observed at 2.36, 2.04, 1.44, and 1.22 Å, which were all within 2% of the value reported for the (1 1 1), (2 0 0), (2 2 0), and (3 1 1) fcc metallic silver reflection (JCPDS No. 1-1167), respectively.

Fig. 6 shows that the UV–vis spectra exhibited peaks at ~400 nm corresponding to the surface plasmon resonance (SPR) absorption of the particles [38]. It can be seen with the polyol con-

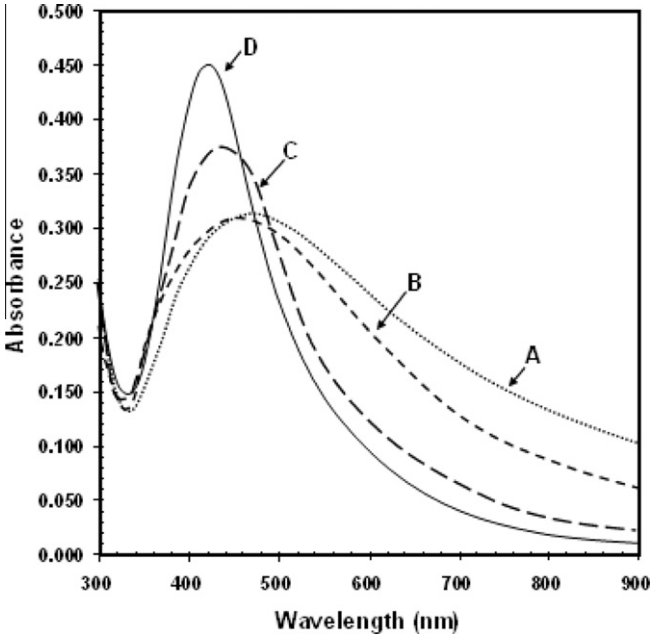

Fig. 6. UV–vis spectra of synthesized silver particles.

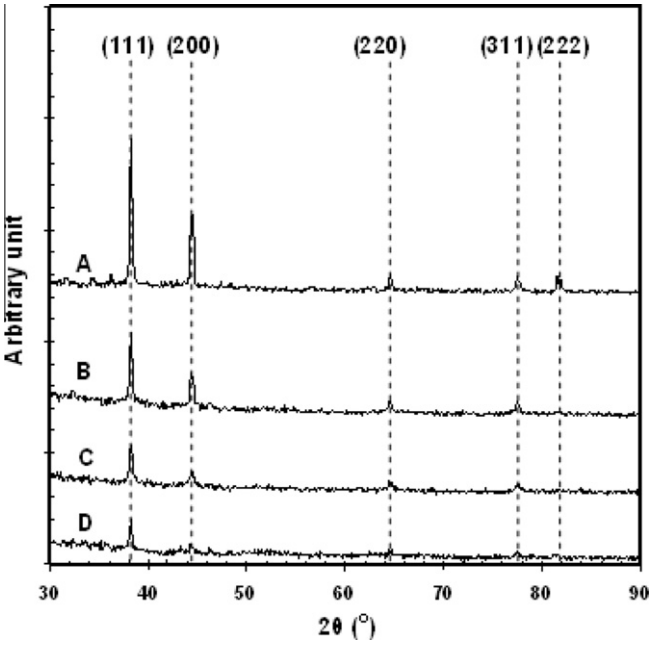

Fig. 7. XRD patterns of the synthesized silver particles.

figurations, the UV–vis spectra show that the absorption intensities of cases C and D were higher than those of A and B, which correlated with Eq. (8) [39]:

$$A_1 = C_{\text{part}} l C_{\text{ext}} / 2.303 \tag{8}$$

where A_1 is the light absorbance, C_{part} is the particle concentration (particles/cm^3), l is the optical path length in nm, and C_{ext} is the extinction cross section for a single particle in nm^2. The absorption peaks shifted positively (red shift) from D ($\sim$ 420 nm) to A ($\sim$ 470 nm), an indication of an increase in the size of the silver particles with different shapes as a result of diffusion growth, aggregation, or a combination of both [40,41].

The symmetry of the absorption peaks C and D was better than those of A and B. Even though case C consisted mostly of spherical particles of a nearly uniform size (shown in Fig. 5c), anisotropic particles were more easily identified than that of D. Therefore, the peak D was the best and its full-width at half-maximum (FWHM) was the smallest, which indicated that silver particles prepared in D were much more uniform in morphology and size. In addition, it is also suggested that for the flake-like particles shown in Fig. 5a (large) and Fig. 5b (small), the absorption peaks could be associated with the larger size of the flat particles [42]. The results were in good agreement with the former TEM analyses.

Fig. 7 shows typical XRD pattern of the as-obtained particle samples. The broadening of the diffraction peaks revealed the nanoscale structure of these samples. Five diffraction peaks could be indexed as (1 1 1), (2 0 0), (2 2 0), (3 1 1), and (2 2 2) planes of the cubic structured metallic silver (JCPDS No. 4-0783). The strong and sharp peaks suggest the formation of highly crystalline silver particles (fcc). The value of the lattice constant was calculated from the spacing distance (d_g) of the (1 1 1) planes and the equation of

$$1/d_g^2 = (h^2 + k^2 + l^2)/a^2 \tag{9}$$

where, h, k, and l are the plane indices, and a is the accurate lattice parameter, $a = 4.0848$ Å, which is consistent with the value of, $a = 4.0862$ Å given by the JCPDS No. 4-0862. The results were in good agreement with the ED analyses. In case A, in particular, the ratio between the intensities of the (2 0 0) and (1 1 1) peaks was higher than usual (0.33 versus 0.25), because of the relative abundance of (1 0 0) facets on the truncated edges of the anisotropic particles [5,43,44]. The average crystallite sizes obtained from each (1 1 1) peak were found to be about 68, 59, 28, and 20 nm for A, B, C, and D, respectively. These approximate values were smaller than the average sizes calculated by TEM image analyses (86, 64, 35, and 21 nm for A, B, C, and D, respectively). As the Scherrer formula always tends to underestimate the real crystallite size [10], this result seemed to favor the hypothesis of the monocrystalline nature of the particles.

The surface areas of the particles as measured by a BET surface area analyzer were found to be about 8.3, 10.8, 22.1, and 26.4 m^2/g for A, B, C, and D, respectively, and the calculation of the surface areas from the XRD patterns was done by the following equation [45]:

$$S_{\text{calc}} = 6 \times 10^4 / td \tag{10}$$

where S_{calc} is the calculated surface area, t is the crystal size in Å, and d is the bulk density of silver. The surface areas from the XRD patterns were about 8.4, 9.7, 20.4, and 28.5 m^2/g for A, B, C, and D, respectively, which matched well with surface areas measured by BET.

In conclusion, the reaction scheme for producing a uniform morphology and dispersity of silver particles using the polyol process involved the following successive reactions: reduction of the soluble silver ions by ethylene glycol, rapid nucleation of silver atoms, and growth of individual nuclei in the presence of a protective agent (PVP) [46,47]. The morphology and size distribution of the particles synthesized from the present work depended strongly on the configuration of the process, and case D produced smaller-sized and more highly monodispersed particles than others. These findings indicate that even though the dependence of the formation characteristics on the reaction temperature and solution injection was considerable, the ultrasonic irradiation could be one of the most critical factors in determining the product features in the method, probably due to the thermal decomposition that occurred at the interfacial region between the cavitation bubbles and the bulk solution and provided reducing radicals [48]. The formation mechanism of the silver particle can be suggested as shown in Eqs. (11)–(16) where RH denotes a PVP or an EG. Eq. (15) refers

to the direct reaction of silver ion with water in the interfacial region between the cavitation bubbles and the liquid [49].

$$H_2O \rightarrow H^{\cdot} + {}^{\cdot}OH \quad (11)$$

$$OH + RH \rightarrow R^{\cdot} + H_2O \quad (12)$$

$$R^{\cdot} + Ag^{+} \rightarrow Ag^{0} + R' + H^{+} \quad (13)$$

$$H^{\cdot} + Ag^{+} \rightarrow Ag^{0} + H^{+} \quad (14)$$

$$Ag^{+} + H_2O \rightarrow Ag^{0} + {}^{\cdot}OH + H^{+} \quad (15)$$

$$nAg^{0} \rightarrow (Ag^{0})_n \quad (16)$$

4. Conclusions

In this study, a novel polyol method to synthesize colloidal silver particles by ultrasonic irradiation was developed. The silver nanoparticles in the presence of ultrasonic irradiation were compared with others from different configurations (at ambient temperature, 120 °C, and 120 °C with injected solutions) in the absence of ultrasonic irradiation in order to obtain systematic results for morphology and size distribution. Even though the temperature of polyol reaction reached only at 80 °C (<120 °C) in the presence of ultrasonic irradiation, a uniform mixing (enhanced collision between silver particle and surrounding components) by ultrasonic irradiation might induce a better formation kinetics and morphological uniformity. The ultrasonic irradiated polyol was proven to be an effective and simple way for the one-step preparation of silver nanoparticles even at ambient temperature and low irradiation frequency (20 kHz) conditions. A further study to verify the particle morphology and size distribution of the silver particles relating to ultrasound parameters (power intensity, irradiation time, etc.) with and without additives is now in preparation to publish elsewhere.

Acknowledgment

This research was supported by the Academic Research Fund of Hoseo University in 2010 (2010-0115).

References

[1] B. Yin, H. Ma, S. Wang, S. Chen, J. Phys. Chem. B 107 (2003) 8898–8904.
[2] D. Kim, S. Jeong, J. Moon, Nanotechnol. 17 (2006) 4019–4024.
[3] X. Jiang, Q. Zeng, A. Yu, Langmuir 23 (2007) 2218–2223.
[4] H. Ma, B. Yin, S. Wang, Y. Jiao, W. Pan, S. Huang, S. Chen, F. Meng, ChemPhysChem 5 (2004) 68–75.
[5] B. Wiley, Y. Sun, B. Mayers, Y. Xia, Chem. Eur. J. 11 (2005) 454–463.
[6] J. Zhu, S. Liu, O. Palchik, Y. Koltypin, A. Gedanken, Langmuir 16 (2000) 6396–6399.
[7] V. Amendola, S. Polizzi, M. Meneghetti, Langmuir 23 (2007) 6766–6770.
[8] H. Jia, W. Xu, J. An, D. Li, B. Zhao, Spectrochim. Acta A 64 (2006) 956–960.
[9] L.-P. Jiang, A.-N. Wang, Y. Zhao, J.-R. Zhang, J.-J. Zhu, Inorg. Chem. Commun. 7 (2004) 506–509.
[10] P.-Y. Silvert, R. Herrera-Urbina, K. Tekaia-Elhsissen, J. Mater. Chem. 7 (1997) 293–299.
[11] H. Xu, K.S. Suslick, ACS Nano 4 (2010) 3209–3214.
[12] W. Zhang, X. Qiao, J. Chen, Mater. Sci. Eng. B 142 (2007) 1–15.
[13] H. Wang, X. Qiao, J. Chen, X. Wang, S. Ding, Mater. Chem. Phys. 94 (2005) 449–453.
[14] C. Feldmann, Adv. Funct. Mater. 13 (2003) 101–107.
[15] C. Feldmann, H.-O. Jungk, Angew. Chem. Int. Ed. 40 (2001) 359–362.
[16] K.S. Suslick, D.A. Hammerton, IEEE Trans. Ultrason Ferroelectr. Freq. Control 33 (1986) 143–147.
[17] R.A. Salkar, P. Jeevanandam, S.T. Aruna, Y. Koltypin, A. Gedanken, J. Mater. Chem. 9 (1999) 1333–1335.
[18] L.H. Thompson, L.K. Doraiswamy, Ind. Eng. Chem. Res. 38 (1999) 1215–1249.
[19] G.W. Lee, J.H. Byeon, Mater. Charact. 60 (2009) 1476–1481.
[20] H.B. Yin, T. Yamamoto, Y.J. Wada, Mater. Chem. Phys. 83 (2004) 66–70.
[21] Z. Lei, Y. Fan, Mater. Lett. 60 (2006) 2256–2260.
[22] S. Brunauer, P.H. Emmett, E. Teller, J. Am. Chem. Soc. 60 (1938) 309–319.
[23] C. Luo, Y. Zhang, X. Zeng, Y. Zeng, Y. Wang, J. Collid, Interface Sci. 288 (2005) 444–448.
[24] M. Tsuji, Y. Nishizawa, K. Matsumoto, M. Kubokawa, N. Miyamae, T. Tsuji, Mater. Lett. 60 (2006) 834–836.
[25] C. Kan, W. Cai, C. Li, L. Zhang, J. Mater. Res. 20 (2005) 320–324.
[26] J. Park, J. Joo, S.G. Kwon, Y. Jang, T. Hyeon, Angew. Chem. Int. Ed. 46 (2007) 4630–4660.
[27] D.T. Robb, V. Privman, Langmuir 24 (2008) 26–35.
[28] D. Wang, C. Song, Z. Hu, X. Zhou, Mater. Lett. 59 (2005) 1760–1763.
[29] M. Tsuji, Y. Nishizawa, M. Hashimoto, T. Tsuji, Chem. Lett. 33 (2004) 370–371.
[30] A.R. Roosen, W.C. Carter, Physica A 261 (1998) 232–247.
[31] Y. Sun, B. Gates, B. Mayers, Y. Xia, Nano Lett. 2 (2002) 165–168.
[32] Z. Zhang, B. Zhao, L. Hu, J. Solid, State Chem. 121 (1996) 105–110.
[33] P.Y. Lim, R.S. Liu, P.L. She, C.F. Hung, H.C. Shih, Chem. Phys. Lett. 420 (2006) 304–308.
[34] P.-Y. Silvert, R. Herrera-Urbina, N. Duvauchelle, V. Vijayakrishnan, K. Tekaia-Elhsissen, J. Mater. Chem. 6 (1996) 573–577.
[35] Y. Sun, Y. Yin, B.T. Mayers, T. Herricks, Y. Xia, Chem. Mater. 14 (2002) 4736–4745.
[36] C. Ducamp-Sanguesa, R. Herrera-Urbina, M. Figlarz, J. Solid, State Chem. 100 (1992) 272–280.
[37] Y. Yin, Z.-Y. Li, Z. Zhong, B. Gates, Y. Xia, S. Venkateswaran, J. Mater. Chem. 12 (2002) 522–527.
[38] T.C. Deivaraj, N.L. Lala, J.Y. Lee, J. Colloid, Interface Sci. 289 (2005) 402–409.
[39] A. Slistan-Grijalva, R. Herrera-Urbina, J.F. Rivas-Silva, M. Ávalos-Borja, F.F. Castillón-Barraza, A. Posada-Amarillas, Physica E 25 (2005) 438–448.
[40] H. Jiang, K.-S. Moon, Z. Zhang, S. Pothukuchi, C.P. Wong, J. Nanopart. Res. 8 (2006) 117–124.
[41] D.A. Andreescu, C. Eastman, K. Balantrapu, D.V. Goia, J. Mater. Res. 22 (2007) 2488–2496.
[42] A. Callegari, D. Tonti, M. Chergui, Nano Lett. 3 (2003) 1565–1568.
[43] Y. Sun, Y. Xia, Science 298 (2002) 2176–2179.
[44] Y. Sun, B. Mayers, T. Herricks, Y. Xia, Nano Lett. 3 (2003) 955–960.
[45] P.K. Khanna, N. Singh, D. Kulkarni, S. Deshmukh, S. Charan, P.V. Adhyapak, Mater. Lett. 61 (2007) 3366–3370.
[46] V.K. LaMer, H.D. Rober, J. Am. Chem. Soc. 72 (1950) 4847–4854.
[47] V.K. LaMer, R.H. Dinegar, J. Chem. Soc. Jpn. 40 (1967) 85–94.
[48] G.-W. Yang, H. Li, Mater. Lett. 62 (2008) 2189–2191.
[49] Y. Nagata, Y. Watananabe, S.-i. Fujita, T. Dohmaru, S. Taniguchi, J. Chem. Soc. Chem. Commun. (1992) 1620–1622.